Check for updates

Identifying Neotectonic Motions in Germany Using Discontinuity-corrected GNSS Data

Nhung Le,[1,2,3] (ID) Benjamin Männel,[1] (ID) Luyen K. Bui,[4,5] (ID) and Harald Schuh[1,2] (ID)

Abstract—The crustal motions throughout Germany have not yet been fully understood because the research scope of previous studies often focuses only on some active grabens. Thus, we investigate it in detail to identify the neotectonic motion characteristics and specific deformation-ongoing regions. High accuracy for monitoring and data analyses is required because the expected crustal deformation in Germany is small. For this reason, we use high-precision GNSS time series processing techniques and interdisciplinary data to reflect actual motions and determine the causes of deformation. Also, an advanced technique of discontinuity correction is introduced to unify the fragments of the GNSS coordinate time series for better velocity field reliability. Our findings show that the crustal motions in Germany tend to increase at a maximum speed of $+1.0$ mm/year. Meanwhile, local subsidence of around -0.8 mm/year is concentrated in the river basins (e.g., the Rhine, Ems, Elbe, Northern Oder, and Danube) and extensive mining regions. The Earth's crust here also behaves with noticeable compressions. The intra-plate motion in Germany is ~ 0.8 mm/year. A special region with an extension rate of $+4.3$ nstrain/year is observed along the North–South trending Regensburg-Leipzig-Rostock shear zone. Machine Learning clusters the 3D plate velocity field in Germany into three distinct regions with increasing speeds: Northwest, East, and Southwest. Significant surface deformations are detected mainly in the Upper Rhine graben, Eifel volcanic field, and Thuringian-Vogtland slate mountains. The harmonic motions of the Earth's crust in Germany have an amplitude of ~ 4.7 mm, in which the surface loads contribute half to this type of motion. The findings will contribute to the overall picture of neotectonics here.

Keywords: Neotectonics, crustal deformation, GNSS, time series analyses, discontinuity-correction technique.

1. Introduction

Germany lies on The Eurasian Plate and has various geological characteristics of the European Cenozoic Rift System (ECRS) (Ziegler, 1992; Meschede and Warr, 2019). The Earth's crust in Germany has experienced tectonic processes like the geologically old East-European Cratonization and the young Alpine-Carpathian Orogen (Raab et al., 2010; Kempe et al., 2017; Strozyk et al., 2017; Meschede and Warr, 2019; Kühne and Weber, 2022). Many studies revealed neotectonic evidence over Germany. For instance, the deep crust layer is comprised of crystalline and sedimentary rocks formed during the Holocene epoch of the Quaternary period (Stosch et al., 1992; Raab et al., 2010; Kushnir et al., 2018; Lehmkuhl et al., 2018; Dill et al., 2020). Germany is not located along an active tectonic boundary, but the build-up and release of tectonic stresses in the upper crust layer result in some noticeable shallow earthquakes (Ziegler, 1992; Meschede and Warr, 2019). The earthquake faults in Germany are concentrated in three major seismotectonic zones: (1) the Rhine area, (2) the Swabian Alb, and (3) the earthquake swarm area of Vogtland (Ritter et al., 2001; Grünthal and Wahlström, 2003; Tyagunov et al., 2006; Rovida et al., 2022; Zeiß et al., 2022). Thus, the ancient geological evidence of crustal motions linked to the active graben structures was also found in these zones, such as the Hohenzollern, Ruhr, Rhine, and Eger grabens (Ziegler, 1992; Ritter et al., 2001; Grünthal and Wahlström, 2003; Tyagunov et al., 2006; Place et al., 2010; Raab et al., 2010; Kempe et al., 2017; Kushnir et al., 2018; Groß et al., 2022; Rovida et al., 2022; Zeiß et al., 2022). In the Northern and central regions of Germany, a few proofs revealed tectonic processes related to fluid-controlled brittle faults, Triassic clastic sediments, and in-situ

[1]   GFZ German Research Centre for Geosciences (Helmholtz-Zentrum Potsdam Deutsches GeoForschungsZentrum GFZ), Potsdam, Germany. E-mail: nhung@gfz-potsdam.de
[2]   Technische Universität Berlin, Berlin, Germany.
[3]   Hanoi University of Natural Resources and Environment, Hanoi, Vietnam.
[4]   School of Earth and Planetary Sciences, Spatial Sciences Discipline, Curtin University, Perth, WA, Australia.
[5]   Faculty of Geomatics and Land Administration, Hanoi University of Mining and Geology, Hanoi, Vietnam.

weathering of granite (Raab et al., 2007; Strozyk et al., 2017; Kunkel et al., 2018; Kneuker et al., 2020). Rabbel et al. (1995) also detected a ∼ 10 km-thick crust layer with P-wave high velocities in the North German basin, typical of the extensional movements of the lower crust intruded by mafic magma during the Caledonian orogeny.

Neotectonics refers to the current tectonic process of the Earth's crust; its monitoring is thus essential for a better understanding of the mechanism of the geodynamics and then identifying deformation-risk regions as well as predicting disasters. Various spatial geodetic techniques (e.g., doppler orbitography and radiopositioning integrated by satellites, very long baseline interferometry, and interferometric synthetic aperture radar) have contributed to monitoring Earth's motions with a wide application spectrum (Campbell and Nothnagel, 2000; Couhert et al., 2018; Bui et al., 2021). Of those, Global Navigation Satellite Systems (GNSS) is one of the most commonly-used methods owing to its advantages in high accuracy and continuous operation with a small temporal interval covering a long period, which is particularly useful for detecting slow-moving deformation in the 3D space (Drewes, 1998; Ge et al., 2006; Yu et al., 2020). However, studies of neotectonics in Germany based on GNSS have mainly focused on several areas associated with the ECRS, such as the Rhine, Eifel, and Alpine foreland regions (Rózsa et al., 2005; Fuhrmann et al., 2013; Kreemer et al., 2020; Pintori et al., 2022). A few investigations have been conducted in regional study areas, including Germany, such as Western Europe and the Euro-Mediterranean (Nocquet and Calais, 2003; Piña-Valdés et al., 2022; Serpelloni et al., 2022). Thus, they did not have a detailed assessment of the crustal deformation in Germany. Little work has been studied throughout Germany with a sparse GNSS network but with a timespan that is not yet long enough for a complete analysis of Earth's surface deformation (Goebell and Wetzel, 2006). So far, there has been a lack of in-depth GNSS-based investigations of neotectonic monitoring over the entire of Germany.

Together with the improvement of deformation monitoring techniques, cutting-edge data processing algorithms are also proposed. A GNSS data processing procedure often includes two main steps: (1) processing raw GNSS observations to derive station coordinates and (2) decomposing the coordinate time series into linear trends and other non-linear components (e.g., Nocquet and Calais (2003), Fuhrmann et al. (2015), Nocquet et al. (2016), Sánchez et al. (2018), Pintori et al. (2022)). An important task is to deal with discontinuities, which refer to sudden changes or shifts in the GNSS coordinate time series. There are two popular approaches for handling this issue in crustal motion velocity computations. The first approach was introduced in Nocquet and Calais ' study 2003, where discontinuities (so-called jumps) were solved by cutting the GNSS time series into segments and then calculating velocities separately for each segment. This results in different velocity vectors for the same station, and thus, a further step of unifying the estimated velocities by constraint conditions must be conducted. This approach was adopted in the piece-wise constant velocity model (i.e., PCVM) invoked in the international terrestrial reference systems (Bevis and Brown, 2014; Altamimi et al., 2016). However, if these constituent velocities are computed from short segments, the reliability of the unified velocity will decrease. In the second approach, the most stable segment of longer than two years and between known antenna changes is selected to determine velocities (Fuhrmann et al., 2015). In this regard, the entire data are not utilized because the observations beyond the considered segment were excluded.

Therefore, our study suggests another approach to solve discontinuities in a GNSS coordinate time series in an auto-correction way, which combines stepwise regressions and auxiliary data to detect and offset discontinuities caused by measurement device changes. In this way, observations of the entire monitoring timespan will be utilized to obtain a consistent velocity field for better capturing the motions of the Earth's crust. We then apply the proposed approach to a dense GNSS network of ∼ 30-km baselines to analyze neotectonics for the whole of Germany.

This article is structured as follows. Section 2 presents experimental data and GNSS processing strategies, in which an explicit description of the discontinuity-correction technique is also included.

Section 3 shows results and discussions about crustal deformations in Germany using the delicately processed coordinate time series. Finally, conclusions and suggestions are summarized in Sect. 4.

2. Data and Methodology

2.1. Data

We collected and processed data (1994-2020) from 503 continuous GNSS stations in Germany from different networks (e.g., IGS,[1] EPN,[2] GREF,[3] and SAPOS[4]). Based on primary investigations from the PPP (Precise Point Positioning) solutions, we selected 346 stations that met strict conditions of deformation monitoring (e.g., accuracy, reliability, and robustness of solutions) for in-depth analyses of crustal movement characteristics (Fig. 1a). The selected stations covered a timespan from 3 to 26 years, among which 276 stations were observed continuously over ten years, accounting for 79.8 % of the total stations.

Additionally, we use the seismic data (i.e., earthquakes), GNSS metadata (e.g., antenna changes or firmware updates), and the data of groundwater extraction and ore mining data to verify discontinuities, anomalies, and subsidence. These auxiliary data are available in the databanks: USGS, GEOFON, Semisys, and BGR. For example, Fig. 1b shows antenna change records obtained from Semisys (Bradke, 2020) for discontinuity corrections in the GNSS time series. The ESMGFZ models are provided by Dill and Dobslaw (2013) to determine the effect of surface loading on the crustal motions in Germany. The links to the data archives are listed in Table 1.

2.2. GNSS Processing Strategies

The tectonic process has been occurring over millions of years, and the Earth's crust is driven by both endogenous and exogenous factors (Oliver,

1991; Hilst and McDonough, 1999; Wessel, 2011). Its motions form a complicated trajectory, including linear and non-linear patterns, as mentioned by Bevis and Brown (2014). Thus, this study focuses on two typical long-term motions: linear trends and harmonic variations. The linear element in the GNSS coordinate time series is the basis for computing crustal motion velocity fields. The tides (both solid Earth and Ocean) contribute to the harmonic motions of the Earth's crust but have been corrected during the network adjustment by the GFZ-EPOS.P8 software, following the IERS conventions (Petit and Luzum, 2010). However, non-tidal loadings (e.g., hydrology, atmosphere, and ocean), causing systematic and significant surface deformations of the Earth's crust (Dill and Dobslaw, 2013; Männel et al., 2019), have not yet been considered while adjusting the GNSS network. To conserve global mass, we also need to consider barystatic sea-level variations, which are not yet accounted for in the oceanic loading model. Moreover, there is no globally unique dominating loading type because the pressure magnitude of loading will depend on (1) the relative position between the monitoring stations and loading sources and (2) the Earth's elasticity. Therefore, this study investigates four surface loadings (hydrology, atmosphere, ocean, and sea level) to determine their effect on the Earth's crust and how far the loadings drive it on a linear trajectory.

The GNSS coordinate time series are obtained from the Network (NET) solutions in the ITRF2014. This study uses nine control stations surrounding Germany (Fig. 1a) selected from the highest accuracy category, based on the station classification criteria in the previous studies (Legrand and Bruyninx, 2020; Le et al., 2022). The strategies of the GNSS network adjustment follow our GFZ-repro3 campaign, which has been described in Männel et al. (2020), Männel et al. (2021). As a continuation, this study will delve into the time series post-processing. Taking advantage of functions in the MATLAB® library, we build an end-to-end workflow of the GNSS time series analyses (Fig. 2), including the discontinuity-correction technique discussed in Sect. 2.3. The program's inputs are the outputs of EPOS.P8 (i.e., the raw GNSS coordinate time series). The derived time series are decomposed by function approximation

---

[1] https://www.igs.org/network.
[2] https://epncb.oma.be/.
[3] https://gref.bkg.bund.de/Subsites/GREF/DE/Home/home.html.
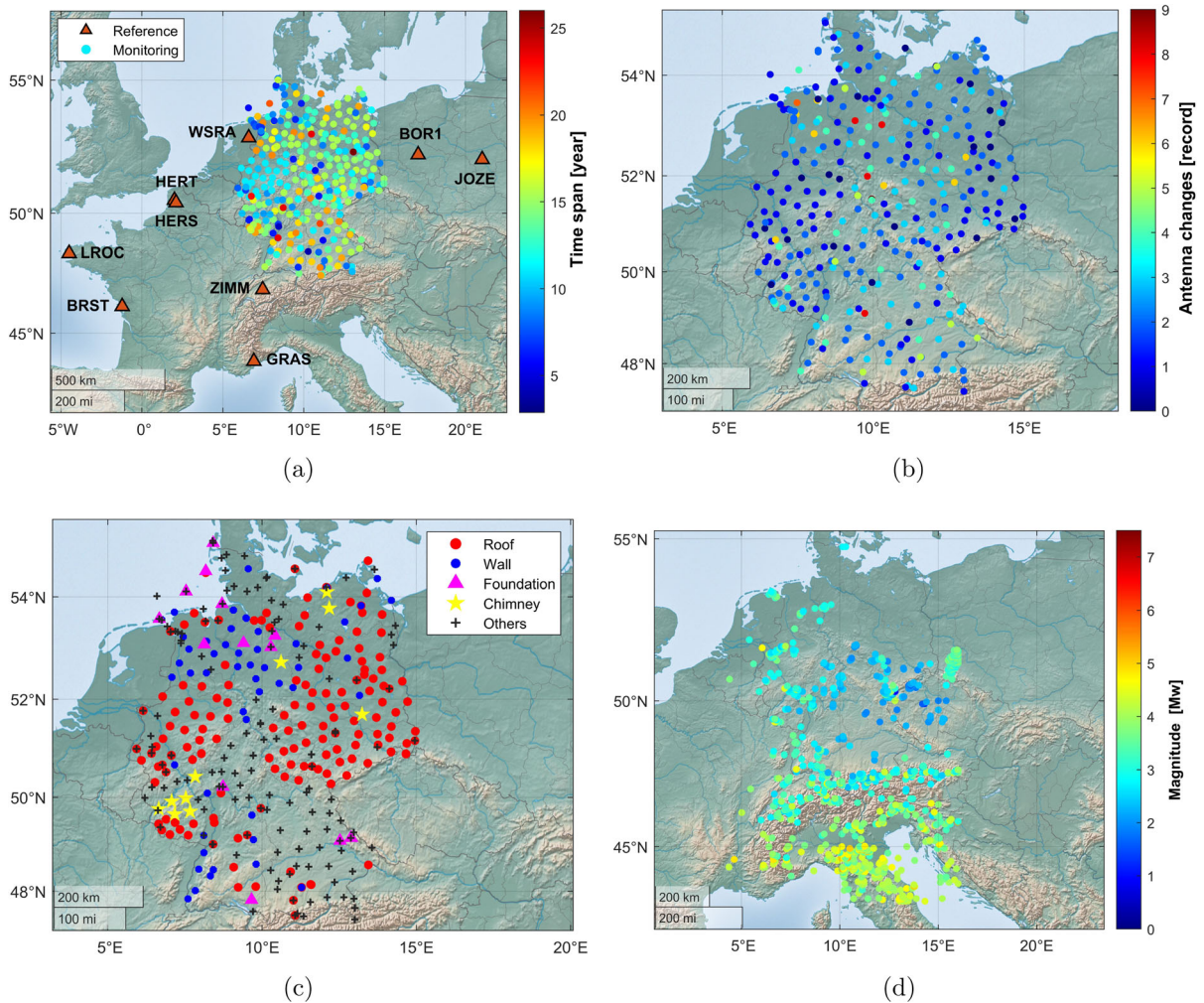[4] https://sapos.de/.

Figure 1
Distribution of the continuous GNSS stations used for investigating the crustal motions (**a**) and the auxiliary data to verify discontinuities and anomalies in the GNSS time series, including antenna changes (**b**), monument description (**c**), and earthquake distribution in the European countries (**d**)

methods and the remove-restore principle, in which a specific element of interest is extracted for further analyses by removing any unrelated characteristics. When all is done, we restore all elements back to the original GNSS time series. Linear regressions are applied to determine linear crustal motions. Then, we fit the GNSS time series to determine nonlinear elements using a combination of sine functions. Ultimately, the output of this program is fine data ready for further analyses.

2.3. Discontinuity-Correction Technique

There are several causes of discontinuities in the GNSS coordinate time series, such as antenna changes (Fig. 1b), earthquakes (Fig. 1d), and the impacts of humans or extreme weather on monuments. Based on the origins, the discontinuities can be divided into two types related to (1) monitoring device changes, which will lead to artificial motions, and (2) seismic events, which likely reflect actual motions of the Earth's crust. Thus, discontinuities that come from the first cause must be corrected.

Table 1

The auxiliary data for correcting discontinuities in the GNSS time series and verifying crustal deformations

Auxiliary data	Databanks	Sources
Earthquakes	GEOFON	https://geofon.gfz-potsdam.de/
	USSG	https://earthquake.usgs.gov/earthquakes/search/
GFZ-GNSS metadata	Semisys	https://semisys.gfz-potsdam.de/
Groundwater and ore extraction	BGR	https://www.deutsche-rohstoffagentur.de/EN
Geophysical fluid loading models	ESMGFZ	https://isdc.gfz-potsdam.de/esmdata/

We filter outliers in the GNSS coordinate time series to avoid biased conclusions due to anomalies. Additionally, using the cleaned GNSS time series can reduce the number of condition loops in distinguishing anomaly values (i.e., outliers or extreme values) from abrupt changes. Accordingly, removing outliers in the GNSS time series will speed up processing. Several popular algorithms, such as moving average (Xiong et al., 2013), generalized extreme studentized deviation (Martel, 2016), quartiles (Vinutha et al., 2018), moving median (Zhang et al., 2019), and Grubbs (Aslam, 2020), can be employed for outlier removal. Among these, the moving median algorithm proved optimal, demonstrating sensitivity to noise while maintaining robustness and unbiased to anomalies (Le et al., 2021). Therefore, it is utilized in this study to filter outliers in all GNSS coordinate time series. The discontinuity-correction technique for the GNSS coordinate time series is performed in two main steps as follows:

In the first step, stepwise regressions are applied to detect abrupt changes and their magnitude in the
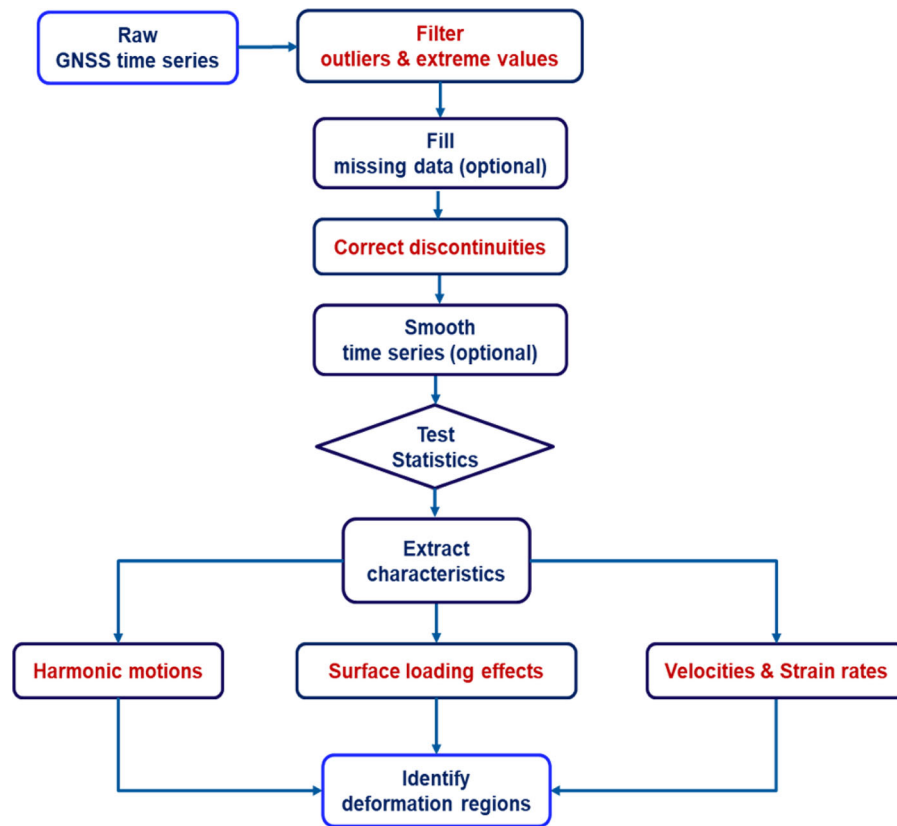

Figure 2
The flowchart of the high-precision GNSS coordinate time series processing

GNSS time series. The antenna change records in the GNSS metadata are used as the priori number of abrupt changes in each time series. If the GNSS metadata is unavailable or the antenna change record equals 0, an alternative mode based on statistical tests, such as ANOVA (Analysis of Variance), between segments in a GNSS time series will be used. This option is embedded in the condition loops of abrupt change detection. The regression process is computed as follows:

$$R(Seg_i) + R(Seg_j) + \tau < R(Seg_{ij})$$

Where τ is the statistical threshold for detecting discontinuities and R (Seg) is the cost function of the regressions corresponding to each segment in the GNSS time series.

It should be noted that we only consider abrupt changes (so-called jumps). Thus, no jumps might be found if its linear trend is steady, even though the harmonic pattern varies considerably. Depending on the characteristics of the GNSS time series, we will opt for the linear regression model or the mean regression model (i.e., regression toward the mean). The linear regression model is selected for the GNSS time series with a strong linear trend. We choose the mean model for the GNSS time series with a weak linear trend. The program detects the most significant changes and then ignores the ones with a magnitude smaller than two times the Root Mean Standard Errors (RMSE) of that GNSS time series (corresponding to a probability of 95 %).

The earthquakes tracked in Germany are minor (please see Fig. 1d), but we would develop algorithms that can also work efficiently on global data. Therefore, this study utilizes seismic data to verify the causes of discontinuities. We use McCue 's 2004 experimental equation to determine GNSS stations located in the earthquake perception radius. A moving window surrounding the mainshocks of the earthquakes helps us identify discontinuities related to these seismic events. The discontinuities might then be skipped after double-checking. This step finishes by distinguishing between the discontinuities caused by device changes and other factors, and the magnitude of the discontinuities is also found.

In the second step, discontinuity-level shifting is implemented based on the nearest neighbour (n). This means that the last observation of the previous segment (Seg$_i$) will merge with the first observation of the next segment (Seg$_j$). The distance to the nearest neighbour depends on the regularity of the measurements. For instance, n = 1 if there is no missing observation. This process is performed from left to right of the GNSS time series by shifting the segments up or down (the blue arrows in Fig. 3).

Notice that this technique can also be applied to converge the antenna centres into one position (for GNSS stations using multi-antennas) or homogeneous two GNSS time series from a former station with an active station. In that case, we only need to tighten the statistical thresholds to ensure that minor abrupt changes will also be detected and corrected. The efficiency of the discontinuity correction will be shown in the following section.

3. Results and Discussions

3.1. Correcting Discontinuities in the GNSS Coordinate Time Series

As mentioned before, outliers in the GNSS time series are first filtered at a 99 % confidence interval by the moving median algorithm. Then, the modified Akima cubic-based interpolated values will replace the observations identified as outliers. Interpolation does not change the accuracy of crustal motion velocity vectors. However, it can avoid losing data and misinformation in the post-audit process (e.g., counting observation records, outliers, jumps, and unobserved days) to contribute to the GNSS metadata and report the final results. We set a three-day moving window surrounding the earthquakes' mainshocks, corresponding to before, on, and after the day the earthquake occurred.

An example of discontinuity correction for the North and Up components of the SAPOS station 0260 in Bavaria is presented in Fig. 3. Clearly, the discontinuities in the GNSS time series deflect the linear trends and then lead to the distortion of the velocity vectors in this station. Five antenna changes are used to set the maximum number of abrupt changes, but three discontinuities in the North and four in the Up are significant. Two small abrupt
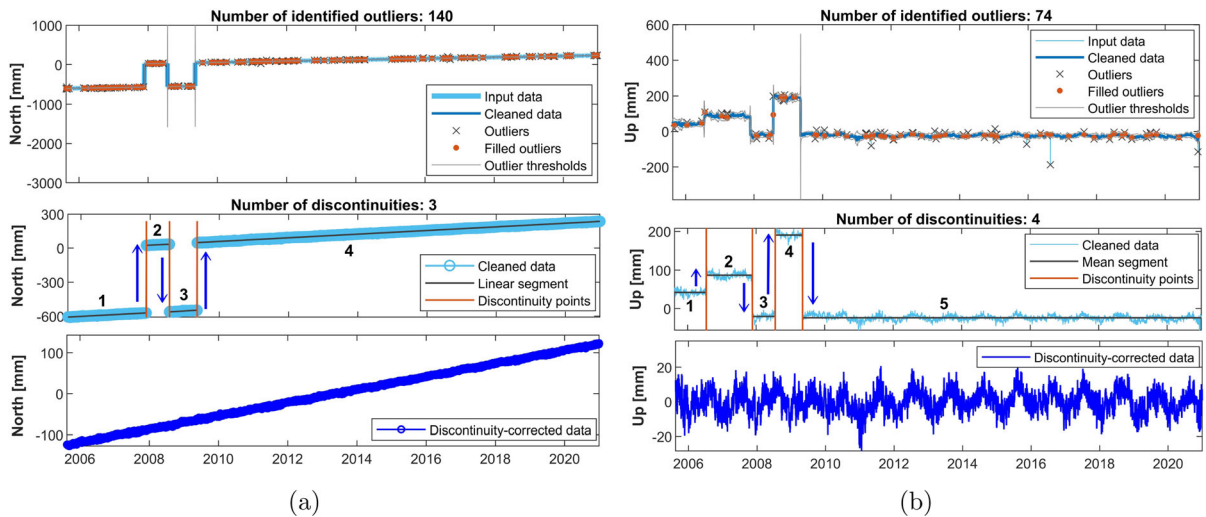
Figure 3

Correcting discontinuities in the North (**a**) and Up (**b**) components of the GNSS coordinate time series at the SAPOS station 0260 in Bavaria

changes skipped are 1.0 and 2.1 mm in the North and Up, while the corresponding maximum discontinuities are $+595.8$ and -211.0 mm. The discontinuity-level shifting is the same way in both the North and Up. For instance, in the North, Segment 1 shifts up $+595.8$ mm to merge with Segment 2 to generate a longer Segment 12. Next, the whole of Segment 12 shifts down by -596.5 mm, to create Segment 123. Similarly, Segment 4 matches Segment 123 by offsetting $+594.4$ mm to merge into a consistent segment (Fig. 3).

The distribution of outliers and discontinuities at the German GNSS stations is displayed in Fig. 4. Almost 85,500 outlier records have been found in three North, East, and Up components, accounting for ~ 1.8 % of the daily coordinate solutions. On average, there are ~ 19 outlier records per station each year. Outliers occur more frequently in Eastern Germany, where antennas are fixed on rooftops (Fig. 1c). In comparison, discontinuities are related to antenna changes rather than the location of the GNSS station installation. This is demonstrated by the correlation between the discontinuities and antenna changes equal to 0.82, while this relationship with receiver changes is only 0.22 (Fig. 5a). There are ~ 2000 abrupt changes detected in all three components of the GNSS time series, in which 1040 discontinuities exceed the statistical thresholds. The number of discontinuities

in the Up component is 546, twice larger than in the North and East (Fig. 5b). This reason can be attributed to how the antenna is mounted on a monument, which can be easily adjusted vertically but not horizontally. The maximum magnitude of the corrected discontinuities is 14,607.25 mm at the SAPOS station 0283 in Mitterteich, occurring on 20 June 2009 (the blue star in Fig. 4b).

Almost 87 % of German GNSS stations have undergone discontinuity corrections (Fig. 5b). More than half of them (shown in yellow in Fig. 5b) have had at least one discontinuity since the installation. The minimum abrupt changes are 0.26, 0.21, and 2.23 mm in the North, East, and Up, respectively. These numbers do not represent much for the algorithm's sensitivity in discontinuity detections (please see the options for defining the maximum number of abrupt changes in Sect. 2.3) but reflect the German GNSS data quality. This finding also advocates the prospect of GNSS for high-precision geodetic applications, especially in horizontal coordinate accuracy that can reach up to ~ 0.3 mm.

More details on the efficiency of time series processing techniques in improving the accuracy of the solution are shown in Table 2. Of these, the median values are determined in a 95 % confidence interval, unbiased by anomalies. The Standard Deviation (SD) mean of the coordinate time series is
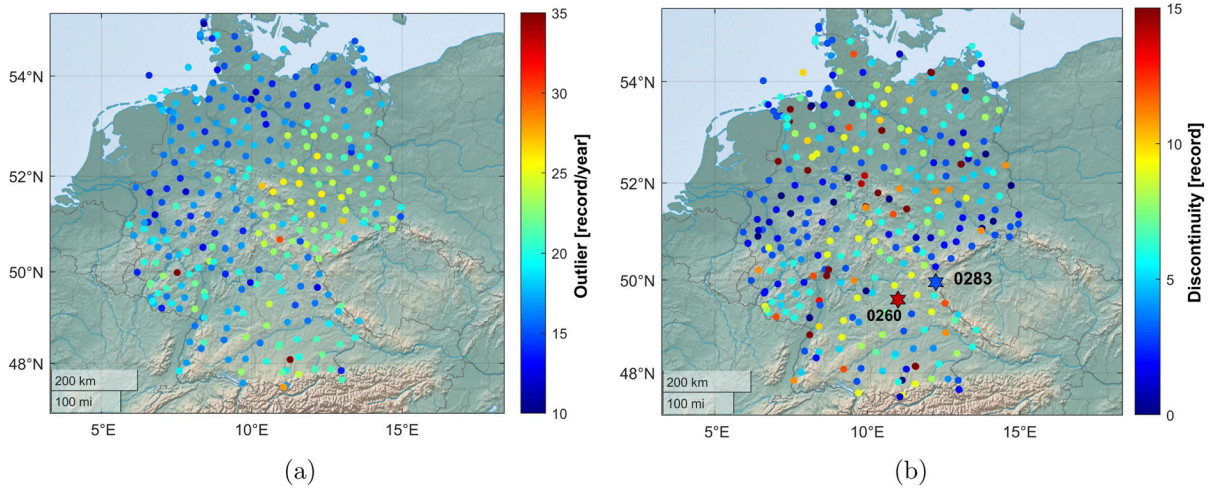
Figure 4
The distribution of outliers (**a**) and discontinuities (**b**) in the GNSS time series at the German monitoring stations
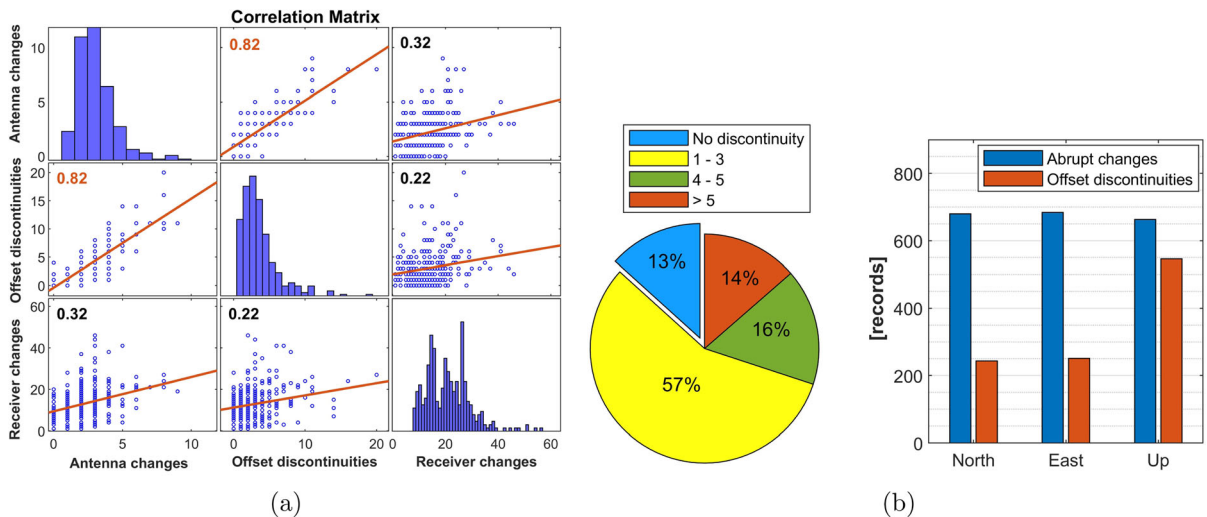

Figure 5
The correlation matrix of the antenna changes, receiver changes, and offset discontinuities (**a**), and the comparison of discontinuity records at the German GNSS stations (**b**)

obtained from the network solutions over the 346 German GNSS stations. The results indicate that thanks to cleaning data and correcting discontinuities, noise in the GNSS coordinate time series (i.e., RMSE) was reduced by 1.5 times. In addition, the velocity vector certainty (i.e., SD) also improves by half. The following steps thereby use these cleaned and discontinuity-corrected time series to identify the crustal motions over Germany.

3.2. Identifying Neotectonic Motion Characteristics in Germany

3.2.1 Linear Motions

Figure 6 shows the *horizontal* velocities and their accuracy based on the NET solutions. The Earth's crust behaves rigidly with an average velocity of ~ 24.6 mm/year toward the Northeastern (Fig. 6a).

Table 2

Estimations of the accuracy of the crustal motion velocities before and after applying the cleaning data and correcting discontinuities

Criteria	NET solutions			Linear regressions											
	SD mean			RMSE (raw)			RMSE (clean+offset)			SD (raw)			SD (clean+offset)		
	North	East	Up	North	East	Up	North	East	Up	North	East	Up	North	East	Up
Median (mm)	0.59	1.02	1.58	2.39	3.60	8.40	1.51	2.32	6.77	0.67	0.97	2.36	0.43	0.62	1.78
Mean (mm)	1.10	1.67	2.57	12.65	11.42	14.37	1.74	2.53	6.88	4.02	3.51	4.46	0.51	0.74	2.04

This movement direction suits the geologically tectonic evidence, such as faults and slips in the Northern Phyllite, Saxothuringian zones, and Alpine molasses (Meschede and Warr, 2019). These motions, often implying the deep crust layer, also steadily follow the general trends of the Eurasian plate found by Kreemer et al. (2014) and Serpelloni et al. (2022). However, relative movements (i.e., intra-plate motions), which are derived by subtracting the ITRF14 plate tectonic model from the GNSS coordinate time series, present non-homogeneous trends (Fig. 6b). In this figure, we excluded eight of the 346 investigated stations whose standard deviations exceeded three times the maximum relative movement. The remaining stations have a monitoring timespan ranging from 4.4 to 26.0 years. The average intra-plate velocity throughout Germany is 0.8 mm/year. The maximum velocity reaches up to 2.6 mm/year at station TGDA in Dagebuell (Hamburg), which was monitored continuously for 8.8 years with 2882 daily records (the red arrow in Fig. 6b). We confirm Nocquet and Calais 's 2003 finding in the Eastern side of the Upper Rhine graben by following their suggestion of using a longer GNSS time series. Here, the Earth's crust is moving with an intra-plate velocity of ~ 0.5 mm/year (based on the observations up to 23.5 years obtained from eight GNSS stations along the Black Forest to Mannheim), a little faster than their result (~ 0.4 mm/year). To avoid a biased interpretation caused by local movements in
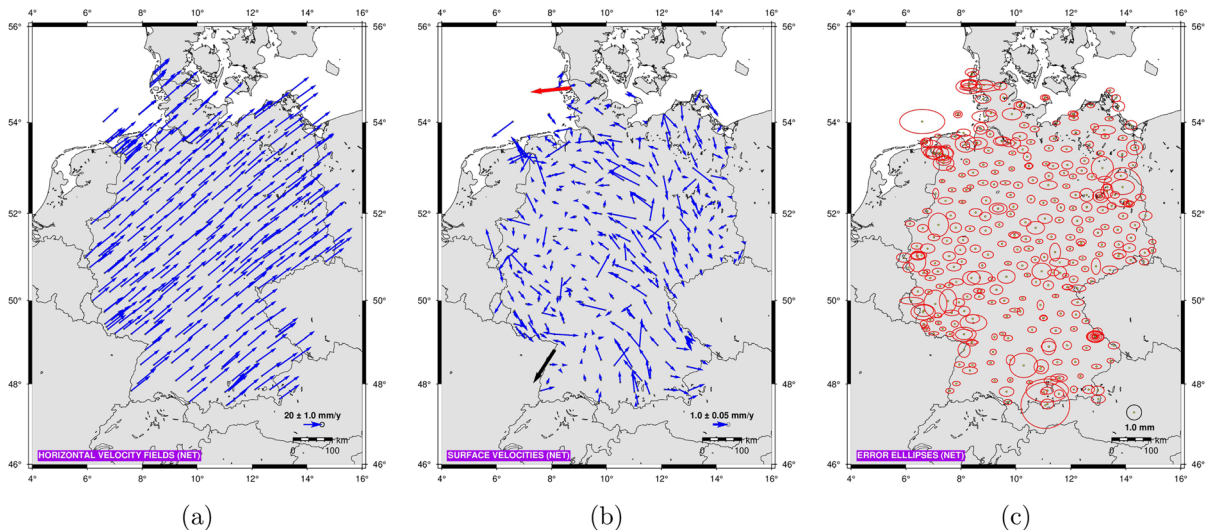

(a)　　　　　　　　　　(b)　　　　　　　　　　(c)

Figure 6
The absolute movement velocity fields using the NET solutions (**a**), the relative movement velocities by subtracting the plate velocity fields of ITRF14 (**b**), the error ellipses of the velocity vectors at a 95 % confidence interval (**c**), and the highlighted velocity vectors of stations TGDA (red) and 0388 (black)

this fault zone, we excluded the SAPOS station 0388, ~ 2.4 mm/year (the black arrow in Fig. 6b), located on the Rheinschleuse Iffezheim dock, as it may have been directly affected by the flow regime of the Rhine river.

The band between $11.5°$ E and $12.5°$ E is of special interest as it moves faster than other regions, with an average speed of ~ 1.0 mm/year. This band is found along the North–South trending Regensburg-Leipzig-Rostock shear zone (Schmidt et al., 2013; Nickschick, 2017). Due to the higher intra-plate movements, this region shows the most significant dilation, with an average rate of $+4.3$ nstrain/year (Fig. 7).

For other regions, the maximum dilatation rate peaks at $+13.5$ nstrain/year in the Northern Alpine foreland. Characterized by compression, the Lower Rhine bay reveals local displacements with a maximum rate of up to -16.4 nstrain/year at $51.5°$ N and

$6.4°$ E. Likewise, the compression signals have been seen noticeably in the typical graben regions, such as the Upper Rhine graben, Swabian Alb, the Ems and Weser river basins, and the borderland with Poland. Our findings provide further and up-to-date information on neotectonics and crustal deformations in Germany, which were just mentioned partly in Reicherter et al. 's 2005; 2008 neotectonic studies.

To estimate the accuracy of the crustal velocities, we use three robust statistic criteria: (1) the SD mean of station coordinates in the NET solutions, (2) the RMSE in linear regressions, and (3) the SD of velocity vectors. These criteria will respond to the velocity vectors' reliability, robustness (in linear regression solutions), and stability. Figure 6d presents the error ellipses of the horizontal velocity vectors (95 % confidence interval) at the 346 GNSS stations. The components of the semi-major and semi-minor axes are computed from the independent
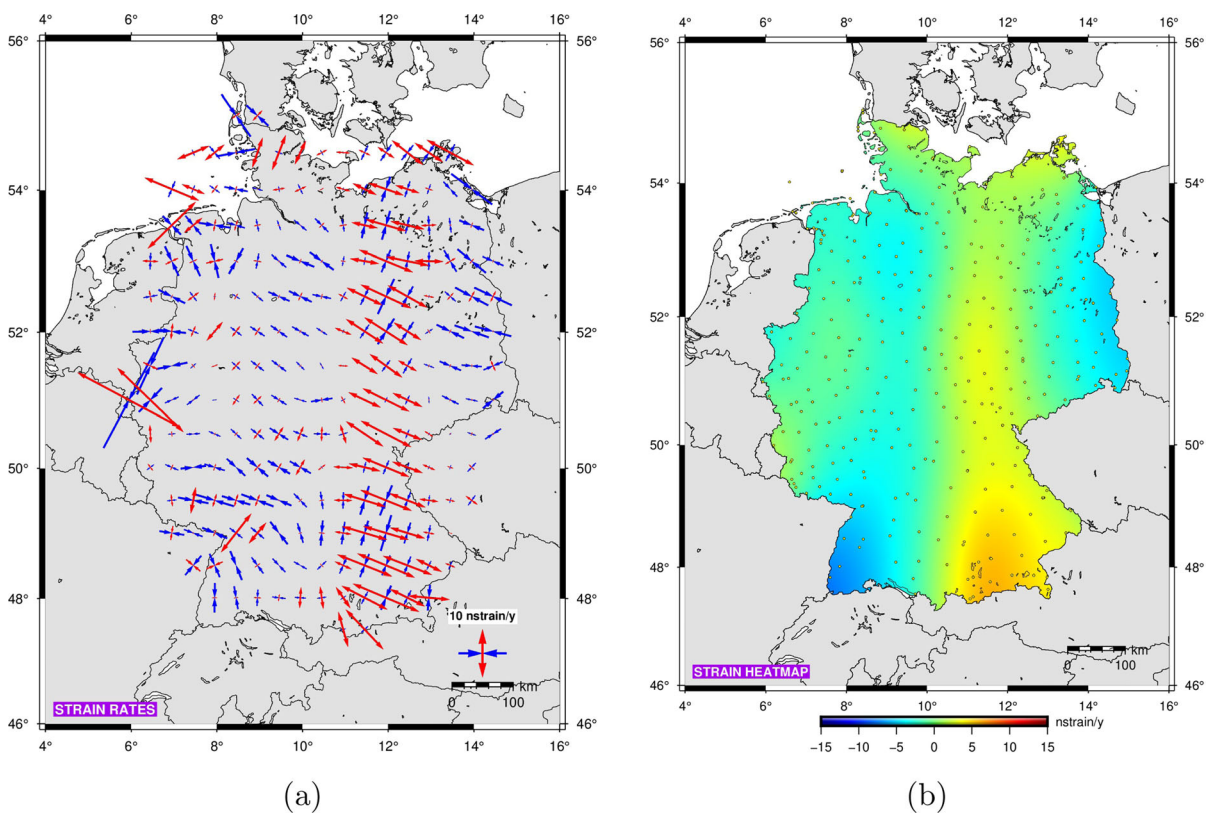

Figure 7
Strain tensors of the Earth's crust, in which (**a**) is strain rates and (**b**) is strain-rate heatmap using the bicubic interpolation algorithm

GNSS coordinate time series, making the correlation of the North and East equal to 0; thus, the rotation angle of the semi-major axes is equal to 90°. The average semi-major axis of the error ellipses is 0.62 mm (<10 % of the absolute crustal movements). Of the investigated stations, 179 show error ellipses with semi-major axes smaller than the intra-plate velocities. The findings demonstrate that all 346 stations match strict conditions in monitoring the absolute movements, and ∼52 % of that can reflect relative movements with high reliability. Considering both the GNSS observation accuracy and intra-plate velocities, changes in crustal motions exceeding random errors can be observed over a monitoring period of three years. We thus recommend updating velocity field maps in Germany after at least five years (so that intra-plate velocities are more significant than two times random errors, corresponding to a 95 % confidence interval).

Regarding *vertical* movements, the velocity fields in Germany show a general uplifting pattern (the red arrows in Fig. 8), in which 136 monitoring sites move with a speed of >0.1 mm/year. Our findings agree with Kreemer et al. 's 2020 in the Eifel region, where the crust moves with a speed of almost +1.0 mm/year (e.g., at stations 0525 and 0526). Furthermore, we also found that uplifts occur in active tectonic regions, such as the Thuringian-Vogtland slate mountains, Saxony, and Alpine foothills (Southern Bayern). The maximum upward movement reaches +1.1 mm/year at the SAPOS station 1657 in Hameln (Lower Saxony) within a monitoring timespan of 6.2 years. In contrast, the significant subsidence with −0.8 mm/year is in Haltern (North Rhine-Westphalia), observed at station 0261 for 10.1 years. It is a fact that the geological feature of the upper crust layer in river basins is mainly formed from the sediment deposition processes, which are often regarded as geologically weak or
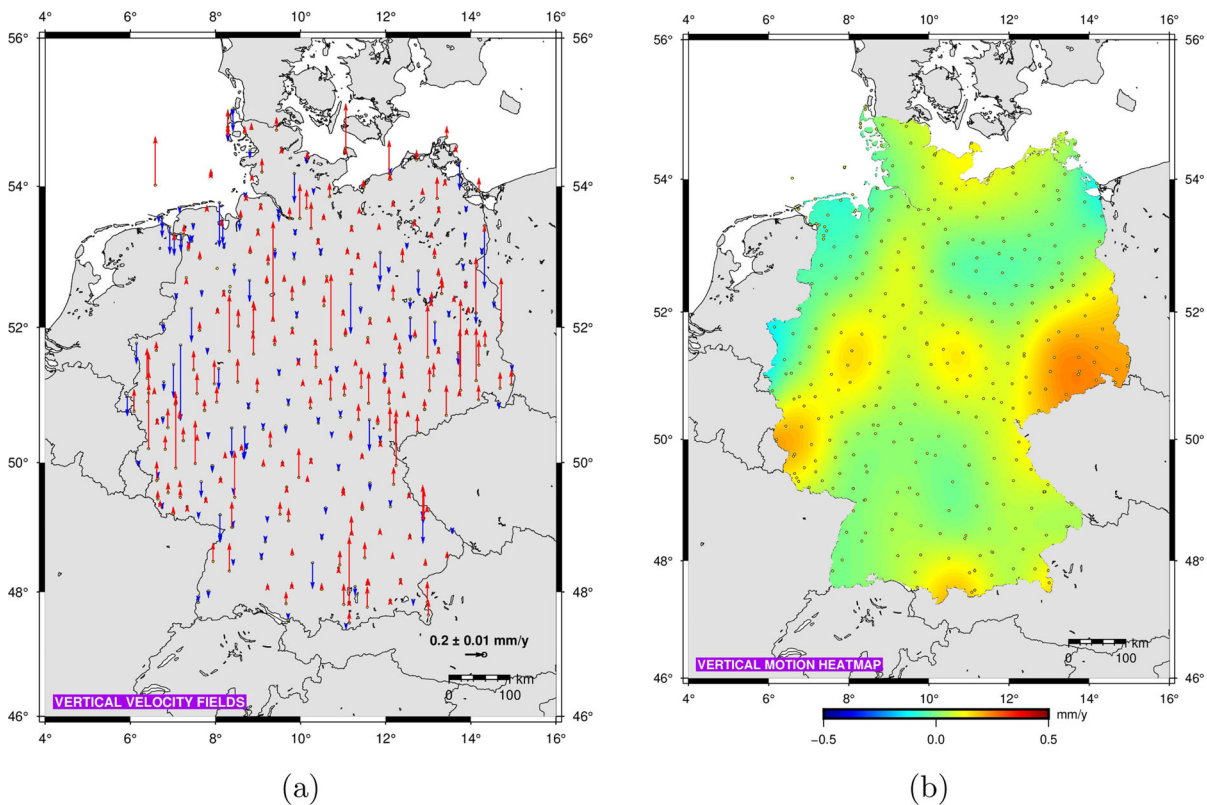

Figure 8
Vertical motion velocity fields using NET solutions (**a**) and the vertical motion heatmap based on the Bicubic interpolation algorithm (**b**)

unstable backgrounds. Proof of this is ongoing subsidence in the river basins, such as the Havel, Elbe, Northern Oder, Rhine, and Ems rivers. Added to this, human activity-related factors, like groundwater extraction and ore mining, also significantly impact the local subsidence mentioned above. The mining data from BRG indicates that some significant subsidence and compression areas (e.g., in Bremerhaven, Lower Saxony, Gransee, and Rheine) are close to groundwater stations and reservoirs or extensive mining regions of gas, petroleum, oil shale, and asphalt.

3.2.2 Harmonic Motions

We apply the function approximation methods by combining sine functions and filtering noise to decompose the non-linear characteristics of the GNSS time series and to determine the harmonic wave parameters (e.g., amplitude, phase, and frequency). Figure 9 describes the non-linear elements, correlations of the GNSS time series at station POTS in Potsdam, and autocorrelation testing by the Ljung-box Q-Test. The wavelet cross-spectrum measures the non-linear correlations between the detrended GNSS time series and the fit models in the North, East, and Up components. The coherence exceeding 0.5 is displayed in arrows. The arrows' orientation aligns with the unit circle's phase delay. For instance, the vertical arrow signifies a phase delay of $\pi/2$ or one-quarter of a cycle for the harmonic wave. The associated time lag depends on the cycle's duration.

The corresponding lag in time depends on the duration of the cycle. Here, we set a spectral frequency in cycles per year (cpy) to identify the harmonic motion characteristics of the Earth's crust.

The spectrum estimations in Figs. 9a and b reveal that the annual variations in the horizontal components are negligible and dominated by noise in the time series. In contrast, a strong positive correlation (r > 0.8) exists between harmonic variations of the Up and the annual sinusoidal pattern. This is indicated via a significant non-linear coherence in the red colour spectrum at a frequency of one year over the monitoring timespan (Fig. 9c). The Up component's semi-annual and annual waves fluctuate around an amplitude of 2.8 and 5.3 mm, respectively. White

noise varies by ~ 2.7 mm, while colour noise flickers with an amplitude of ~ 4.1 mm (Fig. 9d). Additionally, the autocorrelation tests indicate that the variables of the white noise (i.e., the lagged time series in Fig. 9e) do not correlate (shown via r ~ 0). Whereas the flickers generate a downtrend pattern with a high correlation (shown via r ≥ 0.8 for the time series lagged ≤ 5 days). The statistical tests demonstrate that differences in the GNSS station's coordinates within five days are likely because of white noise but not caused by actual motions. This finding implies that using the weekly GNSS coordinate time series can also reflect the harmonic variations of the Earth's crust as adequately as the daily time series.

We conduct the same processing strategies described by station POTS to all the GNSS stations to determine the harmonic motion characteristics of the Earth's crust. The average annual amplitudes corresponding to the three coordinate components are 1.0, 1.2, and 4.7 mm, as seen in Fig. 10. Similar patterns with station POTS, noise dominates the annual characteristics of the horizontal coordinate time series in $\sim 80 \%$ (East) and $\sim 90 \%$ (North) of the investigated GNSS stations. According to the North, East, and Up, the maximum amplitudes of 7.2, 8.2, and 8.8 mm are observed in the Alpine foreland, Northeastern, and Rhine regions, where the GNSS stations are situated in river basins and close to large lakes. Significantly, the annual horizontal variations at SAPOS station 0016 in Gransee (Brandenburg) are more pronounced than the vertical variations, and three coordinate components respond with an amplitude of 7.2, 5.8, and 6.8 mm, respectively. This station is located on a rooftop in an area with a possibly unstable geological background (according to the GFZ-GNSS metadata). It also lies next to Geron Lake and a groundwater station that extracts up to 10 million m³/year (according to BGR[5]). The annual variations of the surface loadings in the vertical direction at this site also exhibit a significant amplitude of 7.6 mm. The most prominent reasons are groundwater flow regimes and water level variations of the Havel River and nearby lakes. The

---

[5] https://www.bgr.bund.de/EN/Themen/Wasser/gw-leiter+ww-d_karte_en.html?nn=1548136.
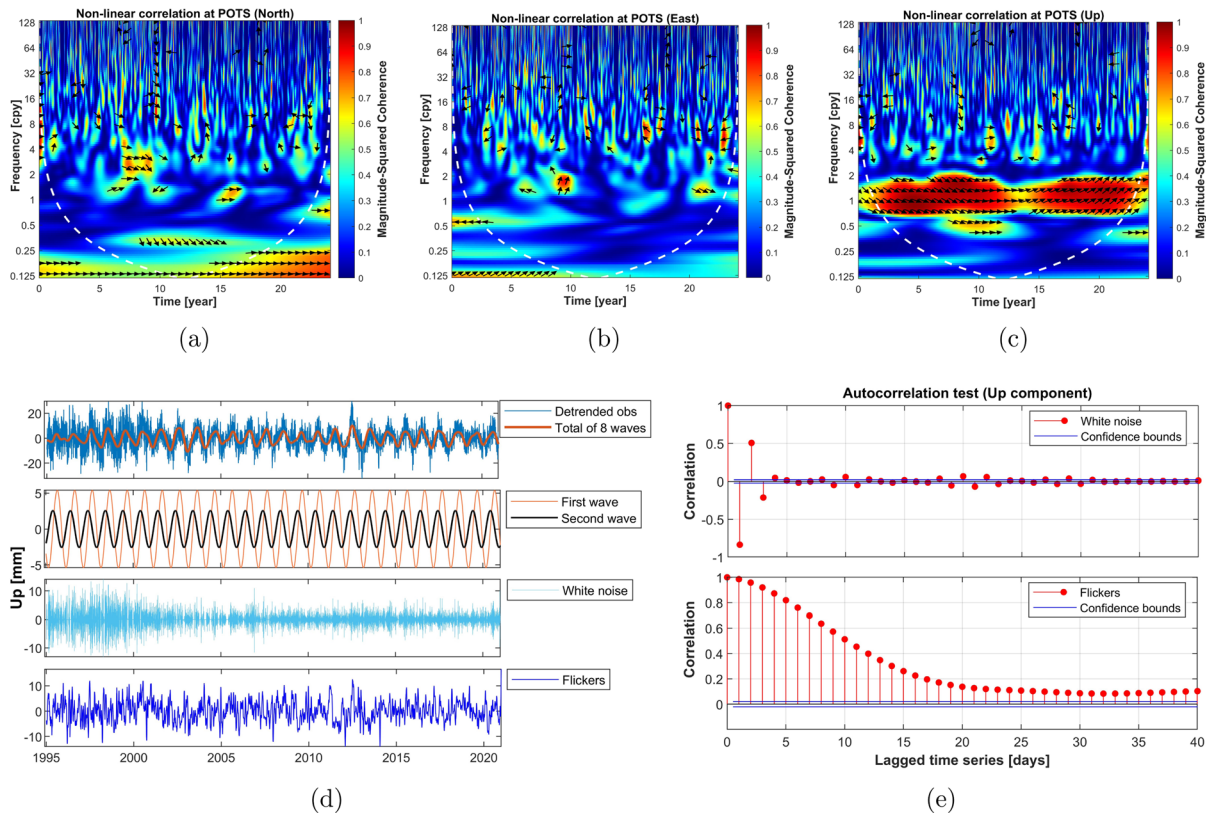
Figure 9
The spectral coherence between the GNSS time series and sine fitting models (i.e., harmonic waves) in the North, East, and Up at station POTS in Potsdam (**a**, **b**, **c**), the non-linear elements (**d**) and autocorrelation tests of white noise and flicker oscillations (**e**) in the Up component

findings point to a close relationship between harmonic crustal motion patterns and water flow mechanisms, as well as the elasticity of the Earth's crust.

3.2.3 Surface Loading Effects on the Crustal Motions

We first regard the loading effects on the harmonic crustal motions. Loading exerting on the Earth's crust in the vertical direction is more significant than the horizontal as the pressure acts perpendicular to the touching surface. Hence, the conclusions hereafter are investigations of the surface loading regimes on the Up component at the monitoring stations throughout Germany. Based on the ESMGFZ models, we determine the annual variations of loadings at the GNSS stations. Among the four investigated loading components, hydrological loading impacts the Earth's surface most significantly, with an annual

amplitude ranging from 3.5 to 5.4 mm. The German Southwestern region along the Rhine river is especially vulnerable. In contrast, the contributions of the sea-level loading (regarding effects due to sea-level changes) and non-tidal ocean loading (primarily driven by the weight and redistributions of ocean water mass) to crustal motions are minor, with an average amplitude of 0.6 and 1.6 mm, respectively. The GNSS stations observed with noticeable variations are concentrated in the German coastal area associated with the North and Baltic seas. Finally, the atmosphere presses the Earth's surface at an amplitude of ∼1.8 mm, and its effect decreases steadily from the Southeastern to the Northwestern regions (Fig. 11).

The annual variation pattern observed at the GNSS stations in Fig. 10 is driven by different factors (i.e., wave sources). Each loading depicted in
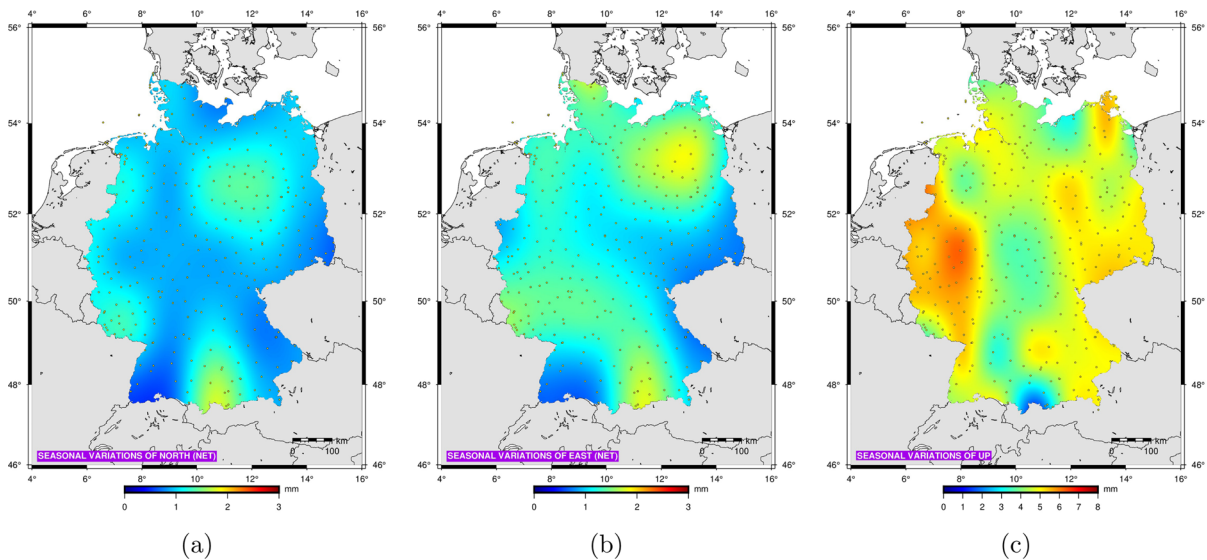
Figure 10
Annual variations of the North (**a**), East (**b**), and Up (**c**) components at the German GNSS stations

Fig. 11 regards a wave source impacting the Earth's crust. Depending on phase differences, the superposition of nonidentical waves can exhibit constructive or destructive interference, which results in an increase or decrease in the total wave amplitude compared to constitutive waves. By subtracting the loading time series from the GNSS coordinate time series, we determine their total impact on the Earth's crust at the monitoring stations. In terms of data characteristics, correcting for the loading effects can considerably reduce annual variations and noise in the Up component of the GNSS time series. That enables improving the velocity field's certainty in the vertical direction. For example, after subtracting the four surface loadings, both the amplitude and noise of the Up decrease significantly. Specifically, the annual amplitude falls from ~ 5.3 to ~ 1.1 mm, and the noise signal reduces from 0.093 to 0.057 dB on a normalized frequency band (Fig. 12a). Furthermore, Pearson's statistical test indicates a strong correlation ($r = 0.88$) between the sinusoidal wave phase in the GNSS time series and total loading (Fig. 12c). As shown on the heatmaps, at most GNSS stations, the annual variations reduce significantly after correcting the loading effect, where the average amplitude decreases from 4.7 to 2.5 mm (Figs. 10c and 12d). In other words, the surface loadings account for half of

the annual variations in the Earth's surface. However, it is also important to emphasize that after removing the loading effect, other periodic variations still remain, but with a smaller amplitude and extended frequency (Fig. 12b). Long-term climate cycle-related factors might cause these variations. Hence, further investigations should be carried out to determine how many factors and how much each factor influences the long-term harmonic motions of the Earth's crust.

Concerning the linear motions, the linear displacements before and after subtracting the surface loadings are described in Fig. 13 and Table 3. The 3D linear trends of the total surface loading in Germany are -0.18, $+0.02$, and $+0.05$ mm/year (Table 3). The loadings drive the crustal motions in a linear trajectory. As shown in Fig. 11, the hydrological loading most significantly impacts the crustal motions. It thus also causes the displacements of the Earth's crust here at the highest level.

The linear trends of the Earth's crust caused by the surface loading are clear and homogeneous. Notably, 79.5 % of the investigated stations moved toward the Southwest (Fig. 13a). In comparison, 72.0 % exhibited a downward trend (Fig. 13b). Throughout the 26-year monitoring period (from 1994 to 2020), the loading caused a displacement of
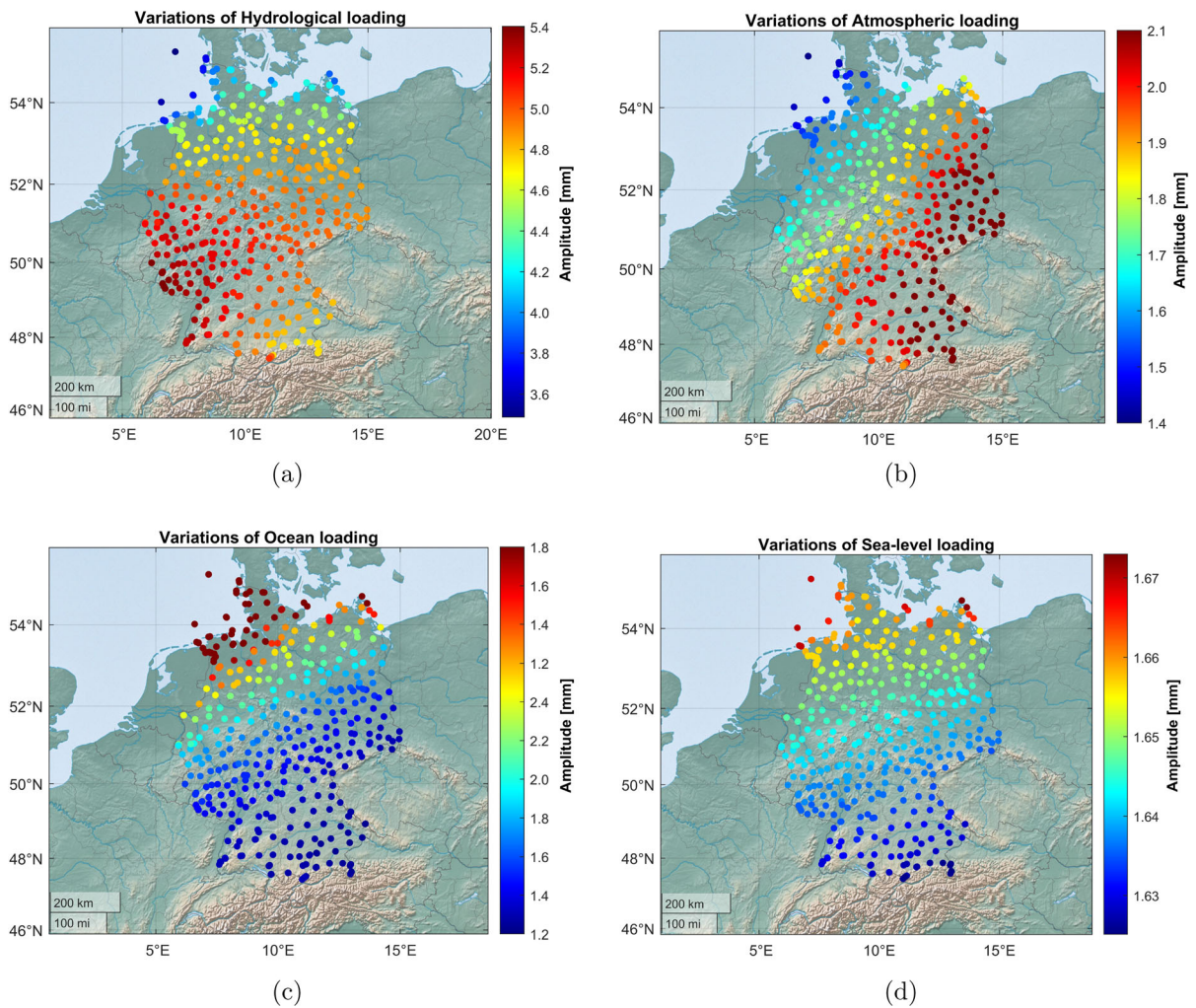
(a)

(b)

(c)

(d)

Figure 11
The effect of the surface loading on the annual variations of the Earth's crust observed at the continuous GNSS stations; in which **a**, **b**, **c**, and d correspond to the hydrological, atmospheric, ocean, and sea-level loadings

roughly 1.8 and 7.5 mm, responding to the horizontal and vertical directions (Table 3). Accordingly, the maximum displacements related to the loadings turn to ~ 0.8 mm/year (North–East) and ~ 1.1 mm/year (Up). Noticeably, these movement modules exceed the average relative crustal motions and are opposite to the absolute crustal motion trends. Nevertheless, the possibility of systematic errors from the surface loading models used in this study is yet to be ruled out. Therefore, investigations on the loading models provided by other research centres should be conducted for a more comprehensive conclusion of the surface loading effect on the Earth's crust.

3.2.4 Clustering of Crustal Motion Major Regions

As indicated above, crustal deformations occur heterogeneously throughout Germany. Thus, we use the unsupervised ML techniques (namely, K-means, Fuzzy C-means, and Hierarchical clustering) to identify major blocks for a better view of the crustal motions here. To implement algorithms, we first normalize the 3D velocities by the Z-score algorithm to avoid biased results due to significant differences in the feature scales. In fact, feature scaling is not always needed for ML techniques. However, this study applies the ML algorithms based on distances

(a)

(b)

(c)

(d)
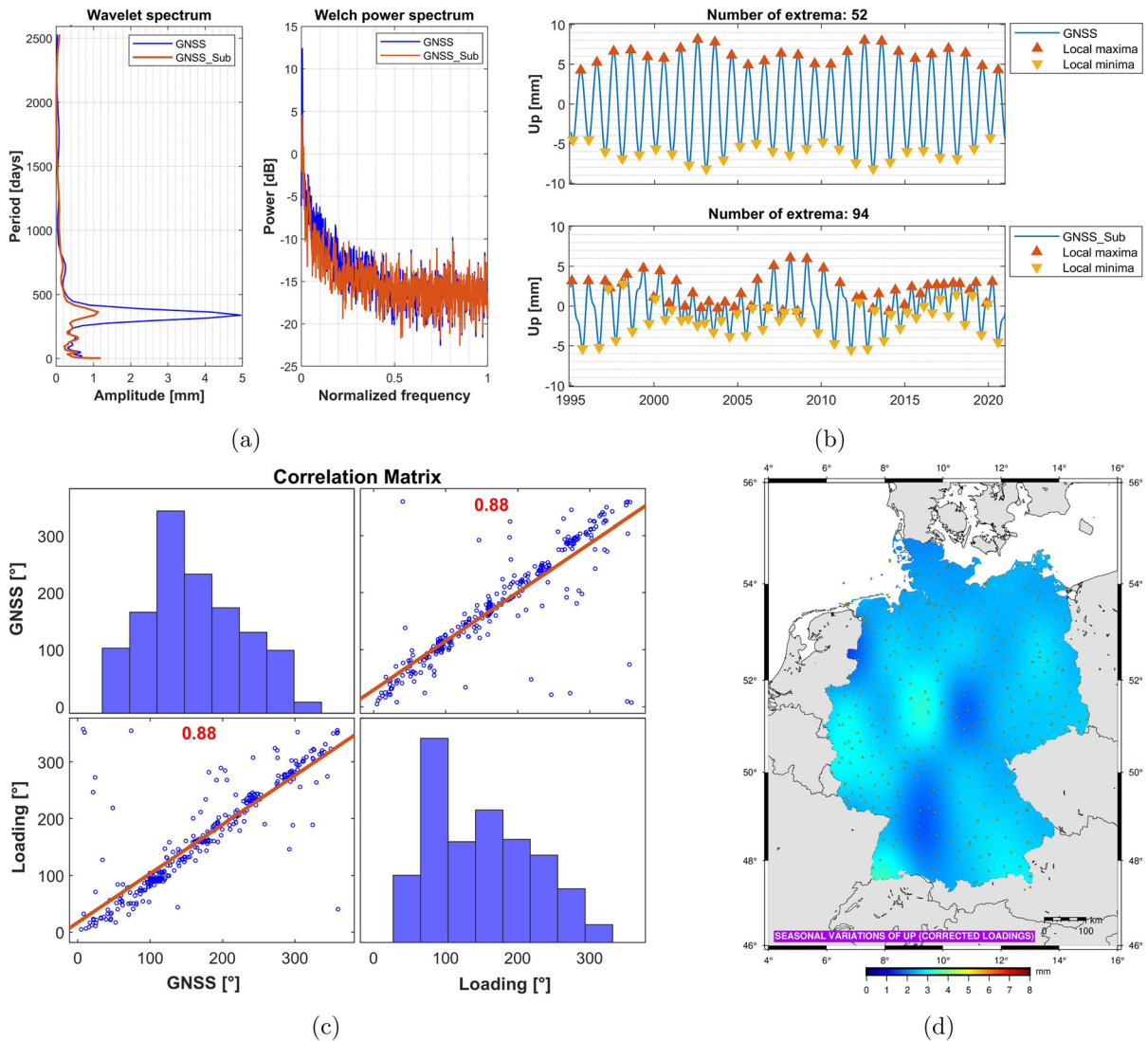
Figure 12

The spectral estimations (**a**) and annual variations (**b**) of the Up component at station POTS before and after subtracting the total loading, Pearson's correlation of the sinusoidal wave phases between the GNSS time series and total loading (**c**), and the annual variation heatmap of the Earth's crust over Germany after correcting the loading effect (**d**)

between data points to determine their similarity of data characteristics for clustering the features into distinct groups. Meanwhile, the horizontal velocities remain at a range of tens of mm/year compared to only a few mm/year for the vertical velocities. Thus, scaling features before clustering the 3D velocity field is recommended for better identifying crustal deformation regions.

Then, we test the velocity clusters' consistency (C) by linkage trees, where velocity correlation is computed in the Euclidean distance. A higher C value presents a lower ambiguity among clusters. For example, the 3D velocity field behaves at C of 0.81 (Fig. 14a), which implies a significant difference among the clustered velocity groups. The y-axis displays the Euclidean distance of the linkages. The relative height of linkage trees or the width of the
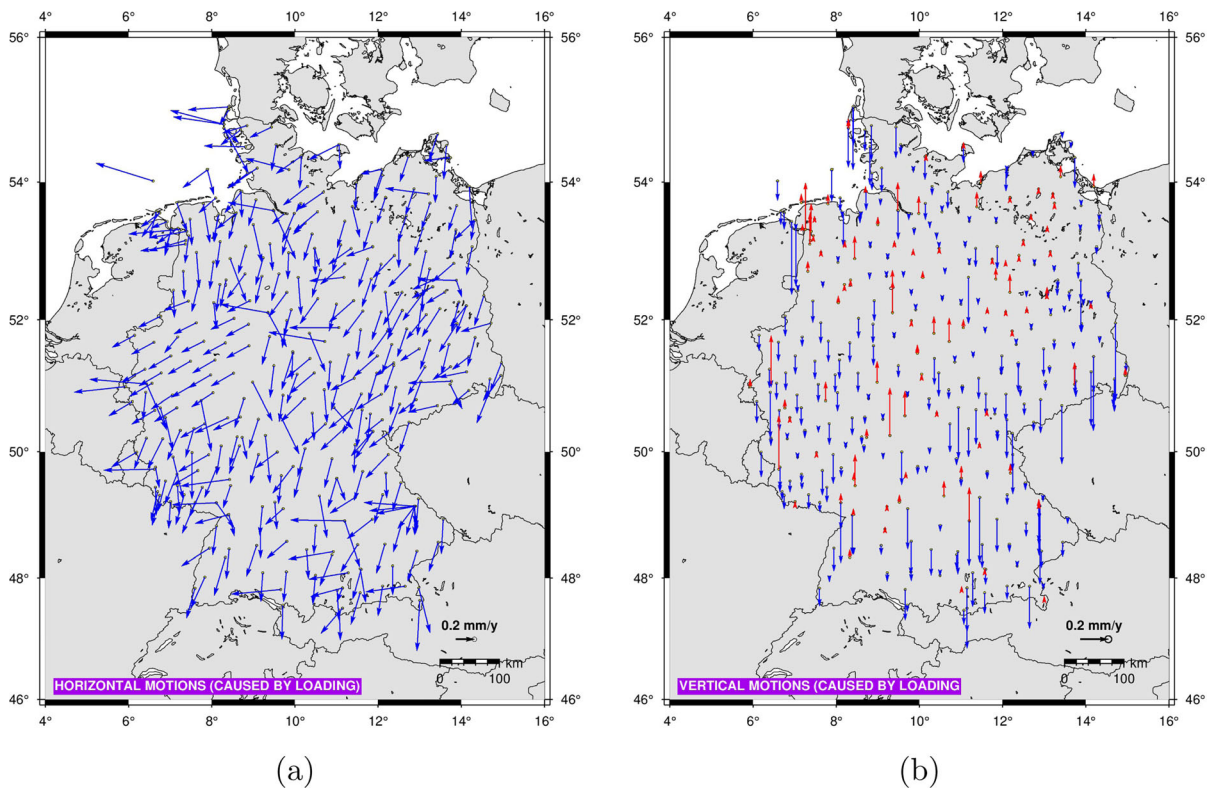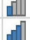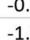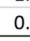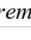
Figure 13
The total loading effect on the linear motions of the Earth's crust in the horizontal (**a**) and vertical (**b**) directions

cutoff thresholds measured on the y-axis shows the consistency of clusters. The F values are fuzzy boundaries between two linkages. In the case of clustering into three groups, the lower and upper boundaries are defined by the cutoff thresholds ranging from 8.7 to 14.5. The linkage trees show a high accuracy in clustering the 3D velocity field into three groups, with an Euclidean distance of ~ 5.7 (i.e., the difference between F2 and F3). Similarly, in the case of clustering velocities into two categories, this distance is ~ 6.7, corresponding to the difference between F1 and F2. By contrast, it is very fuzzy in the case of clustering into smaller groups, where this number stays at ~ 0.2 for four clusters and ~ 1.1 for five clusters. In short, increasing the number of clusters also increases the ambiguity among the clusters. Thus, together with the manifestation of crustal displacement revealed via the above investigations, we set the number of clusters equal to three to determine crustal deformation regions.

There is a high agreement in clustering deformation major regions among the three investigated methods (Fig. 14b). The velocity discrepancy mainly follows the characteristics of the horizontal motion rather than the vertical motion (Fig. 14c). Figure 14d shows the 3D velocity field clustered by processing optimization on the three ML algorithms: K-means, C-means, and Hierarchy. The average NEU velocities corresponding to the three clusters are 25.0 (red), 24.9 (green), and 23.8 mm/year (blue). Accordingly, the Southwest region, covered by Cluster 1, moves with the fastest plate motion velocity while Cluster 3, corresponding to Northwest Germany, remains at the slowest motion level. Along the boundaries of clusters often exhibit a higher possibility of deformations due to the significant differences in movement characteristics (e.g., direction, magnitude, and speed). Notice that, according to the velocity means of the clusters, these three central points can be considered as the Euler reference sites for the local motions in Germany.

Table 3

Velocity fields before (NET) and after (NET-Sub) subtracting the total surface loading

Velocity (mm/yr)	NET			NET_Sub			Loading			Difference		
	North	East	Up	North	East	Up	North	East	Up	North	East	Up
Median	15.64	18.99	0.03	15.86	19.16	0.08	-0.18	0.02	0.05	-0.28	-0.10	-0.04
Mean	15.55	19.00	0.06	15.79	19.14	0.12	-0.18	0.02	0.05	-0.24	-0.14	-0.07
Max (magnitude)	19.08	21.67	1.06	19.23	21.61	1.11	-0.20	0.04	0.08	-0.54	-0.61	-1.06
Min (magnitude)	11.94	14.68	0.00	12.12	14.75	0.00	-0.18	0.00	0.00	0.00	0.00	0.00

Note: Median values are determined in a confidence interval of 95 %, which are unbiased by extreme values

The adjoining regions between different clusters (i.e., the North–South trending Regensburg-Leipzig-Rostock shear zone, Thuringian-Vogtland slate mountains, and Saxo-Thuringian zone) reveal evidence of noticeable deformations. The deformation regions found by ML provide additional evidence for the aforementioned results in intra-plate velocities (Fig. 6b), strain rates (Fig. 7), and vertical crustal movements (Fig. 8).

4. Conclusions and Recommendations

Together with employing unsupervised ML techniques, this study conducted high-precision GNSS time series analysis methods in an end-to-end workflow. Below are the main conclusions and recommendations:

Our study has introduced a discontinuity-correction technique to determine a consistent velocity field over the monitoring period. This technique can also distinguish between seismic-related actual motions and pseudo displacements caused by changes in GNSS devices. Following the proposed workflow of crustal motion analyses, the findings reveal that the Earth's crust in Germany is stable, exhibiting an average intra-plate velocity of ≤ 1.0 mm/year. The vertical displacement is small and generally generates an upward pattern, especially in active motion regions, where velocities can reach up to $+1.0$ mm/year. Subsidence of ~ 0.8 mm/year occurs in the river basins in Germany, centralized mining regions, and the Upper Rhine graben, where strong compressions are also indicated. The highest extension region of $11.5°$ E to $12.5°$ E stretches along the Regensburg-Leipzig-Rostock shear zone with an average strain rate of $+4.3$ nstrain/year. Found by ML, the areas

particularly vulnerable to deformations are Southwestern Germany and the lowlands of the Havel and Elbe rivers. In addition, harmonic motions show annual variations with an amplitude of ~ 4.7 mm. The surface loadings considerably impact both the nonlinear and linear motions of the Earth's crust, in which the hydrological loading forces exert at the highest level. Based on the characteristics of crustal motions in Germany and the accuracy of GNSS observations, updating velocity field maps after at least five years is recommended.

Germany has an evenly distributed GNSS network, but most stations are built for multi-purposes. For the convenience of monitoring and maintenance, the stations are mainly located on constructions (e.g., chimneys, rooftops, and walls). These installations might cause a local monument displacement and increase data post-processing complexity. Moreover, it is a fact that GNSS-based height positioning is still challenging in high-precision deformation monitoring. For cross-validations, it is necessary to establish integrated geodetic networks (e.g., the combination of GNSS, InSAR, and leveling) for tracking crustal motions. In which the monitoring stations should be installed on rock basements along geological traces (e.g., the Eifel volcanic field, Albstadt, Regensburg-Leipzig-Rostock shear, Upper Rhine graben, and river basins).
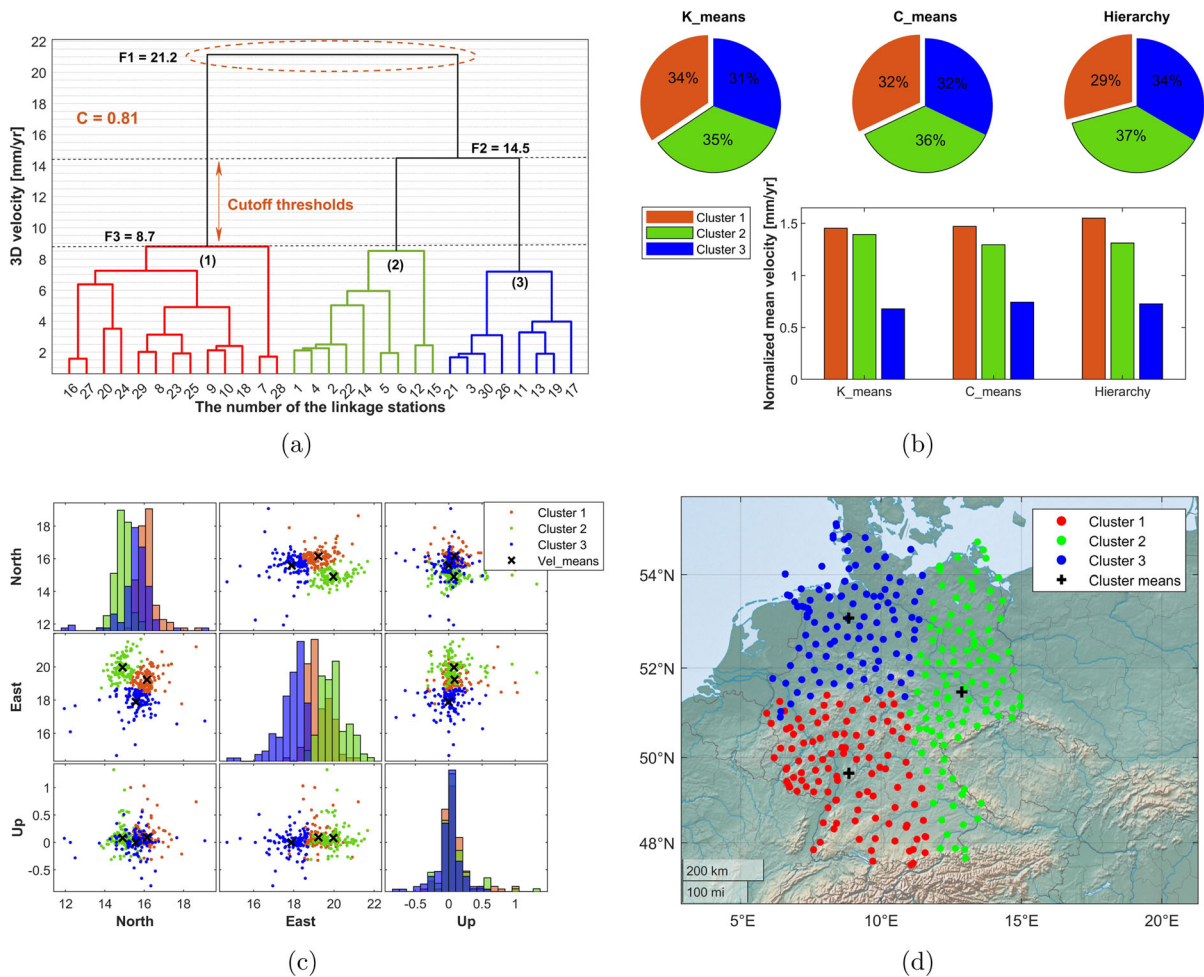
(a)

(b)

(c)

(d)

Figure 14

Clustering of the NEU velocity field using Machine Learning, including 2D distributions of clustered velocities (**a**), 3D distributions of clustered velocities (**b**), the dendrogram of cluster linkage (**c**), and the clustered GNSS stations (**d**)

German satellite positioning service (SAPOS®); the Earth System Modelling group in Section 1.3, GFZ Potsdam, Germany; the German Federal Institute of Hydrology (BFG); the German Federal Agency for Cartography and Geodesy (BKG); the German Federal Institute for Geosciences and Natural Resources (BGR) in Hanover; the Central European Volcanic Province Observatory (CVO); the GEOFON seismic program in the GFZ Potsdam, Germany; and the USGS Earthquake Hazards Program in the US; for providing the GNSS data, loading models, and validation data. We have taken advantage of the Machine Learning toolboxes and functions in the MATLAB® library (Release 2022a) to code the computation programs for implementing the algorithms in this study. Besides, we also benefited from the open-code sources in Python and Bash scripts provided by Anastasiou et al. (2018) to compute strain rates and visualize the GMT maps.

Author Contributions BM and NL designed the study. NL coded the computation program to implement the algorithms, processed data, and interpreted the results. BM, LB, and HS verified the results. NL wrote the manuscript, and all the authors revised it for the article preparation.

Funding

Open Access funding enabled and organized by Projekt DEAL. The authors have not disclosed any funding.

Data Availability

The data of the GNSS coordinate time series and velocity fields in Germany can be made available upon request. The data of the surface loadings at the corresponding GNSS stations can be accessed from the Information System and Data Center for Geoscientific Data (ISDC) on the GFZ website: https://isdc.gfzpotsdam.de/homepage/.

Declarations

Conflict of interest The authors declare that they have no competing interests.

Publisher's Note Springer Nature remains neutral with regard to jurisdictional claims in published maps and institutional affiliations.

REFERENCES

Altamimi, Z., Rebischung, P., Métivier, L., & Collilieux, X. (2016). ITRF2014: A new release of the International Terrestrial Reference Frame modeling nonlinear station motions. *Journal of Geophysical Research: Solid Earth, 121*(8), 6109–6131. https://doi.org/10.1002/2016JB013098

Anastasiou, D., Papanikolaou, X., Ganas, A., & Paradissis, D. (2018). StrainTool: A software package to estimate strain tensor parameters. *Zenodo.* https://doi.org/10.5281/zenodo.3239497

Aslam, M. (2020). Introducing Grubbs's test for detecting outliers under neutrosophic statistics—an application to medical data. *Journal of King Saud University-Science, 32*(6), 2696–2700. https://doi.org/10.1016/j.jksus.2020.06.003

Bevis, M., & Brown, A. (2014). Trajectory models and reference frames for crustal motion geodesy. *Journal of Geodesy, 88*(3), 283–311. https://doi.org/10.1007/s00190-013-0685-5

Bradke, M. (2020). SEMISYS–sensor meta information. *System.* https://doi.org/10.5880/GFZ.1.1.2020.005

Bui, L. K., Le, P. V., Dao, P. D., Long, N. Q., Pham, H. V., Tran, H. H., & Xie, L. (2021). Recent land deformation detected by Sentinel-1A InSAR data (2016–2020) over Hanoi, Vietnam, and the relationship with groundwater level change. *GIScience and Remote Sensing, 58*(2), 161–179. https://doi.org/10.1080/15481603.2020.1868198

Campbell, J., & Nothnagel, A. (2000). European VLBI for crustal dynamics. *Journal of Geodynamics, 30*(3), 321–326. https://doi.org/10.1016/S0264-3707(99)00068-X

Couhert, A., Mercier, F., Moyard, J., & Biancale, R. (2018). Systematic error mitigation in DORIS-derived geocenter motion. *Journal of Geophysical Research: Solid Earth, 123*(11), 10142–10161. https://doi.org/10.1029/2018JB015453

Dill, H., Buzatu, A., Balaban, S., Ufer, K., Techmer, A., Schedlinsky, W., & Füssl, M. (2020). The transition of very coarse-grained meandering to straight fluvial drainage systems in a tectonized foreland-basement landscape during the Holocene (SE Germany)—a joint geomorphological-geological study. *Geomorphology, 370,* 107364. https://doi.org/10.1016/j.geomorph.2020.107364

Dill, & Dobslaw. (2013). Numerical simulations of global-scale high-resolution hydrological crustal deformations. *Geophysical Research: Solid Earth, 118*(9), 5008–5017. https://doi.org/10.1002/jgrb.50353

Drewes, H. (1998). Combination of VLBI, SLR and GPS determined station velocities for actual plate kinematic and crustal deformation models. *International Association of Geodesy Symposia.* https://doi.org/10.1007/978-3-642-72245-5_59

Fuhrmann, T., Heck, B., Knöpfler, A., Masson, F., Mayer, M., Ulrich, P., & Zippelt, K. (2013). Recent surface displacements in the Upper Rhine Graben—preliminary results from geodetic networks. *Tectonophysics, 602,* 300–315. https://doi.org/10.1016/j.tecto.2012.10.012

Fuhrmann, T., Knöpfler, A., Mayer, M., Schenk, A., Westerhaus, M., Zippelt, K., & Heck, B. (2015). An inventory of surface movements in the upper Rhine graben area southwest Germany from SAR-interferometry GNSS and precise levelling. *International Association of Geodesy.* https://doi.org/10.1007/1345_2015_116

Ge, M., Gendt, G., Dick, G., Zhang, F. P., & Rothacher, M. (2006). A new data processing strategy for huge GNSS global networks. *Journal of Geodesy, 80*(4), 199–203. https://doi.org/10.1007/s00190-006-0044-x

Goebell, S., & Wetzel, H. U. (2006). Contributions to the deformation analysis in Germany based on precise and continuous GPS measurements. *Natural Hazards, 38*(1–2), 177–197. https://doi.org/10.1007/s11069-005-8612-6

Groß, P., Pleuger, J., & Handy, M. R. (2022). Rift-related paleogeography of the European margin in the Eastern Alps (Central Tauern Window). *Swiss Journal of Geosciences.* https://doi.org/10.1186/s00015-022-00426-9

Grünthal, G., & Wahlström, R. (2003). An Mw based earthquake catalogue for central, northern and northwestern Europe using a hierarchy of magnitude conversions. *Journal of Seismology, 7*(4), 507–531. https://doi.org/10.1023/B:JOSE.0000005715.87363.13

Hilst, R. V. D., & McDonough, W. (Eds.). (1999). *Composition, deep structure and evolution of continents*. Elsevier Science. https://doi.org/10.1016/S0419-0254(99)80001-9

Kempe, S., Bauer, I., & Glaser, S. (2017). In A. Klimchouk, A. N. Palmer, J. D. Waele, A. S. Auler, & P. Audra (Eds.), *Hypogene caves in Germany, geological and geochemical background.* Springer. https://doi.org/10.1007/978-3-319-53348-3

Kneuker, T., Blumenberg, M., Strauss, H., Dohrmann, R., Hammer, J., & Zulauf, G. (2020). Structure, kinematics and composition of fluid-controlled brittle faults and veins in Lower Cretaceous claystones (Lower Saxony Basin, Northern Germany): Constraints from petrographic studies, microfabrics, stable isotopes and biomarker analyses. *Chemical Geology, 540*, 119501. https://doi.org/10.1016/j.chemgeo.2020.119501

Kreemer, C., Blewitt, G., & Davis, P. M. (2020). Geodetic evidence for a buoyant mantle plume beneath the Eifel volcanic area, NW Europe. *Geophysical Journal International, 222*(2), 1316–1332. https://doi.org/10.1093/gji/ggaa227

Kreemer, C., Blewitt, G., & Klein, E. C. (2014). A geodetic plate motion and global strain rate model. *Geochemistry, Geophysics, Geosystems.* https://doi.org/10.1002/2014GC005407

Kühne, O., & Weber, F. (2022). *Germany Geographies of Complexity*. Springer Nature Switzerland AG. https://doi.org/10.1007/978-3-030-92953-4

Kunkel, C., Aehnelt, M., Pudlo, D., Kukowski, N., Totsche, K. U., & Gaupp, R. (2018). Subsurface aquifer heterogeneities of Lower Triassic clastic sediments in central Germany. *Marine and Petroleum Geology, 97*, 209–222. https://doi.org/10.1016/j.marpetgeo.2018.06.022

Kushnir, A. R., Heap, M. J., Baud, P., Gilg, H. A., Reuschlé, T., Lerouge, C., & Duringer, P. (2018). Characterizing the physical properties of rocks from the Paleozoic to Permo-Triassic transition in the Upper Rhine Graben. *Geothermal Energy.* https://doi.org/10.1186/s40517-018-0103-6

Le, N., Mannel, B., Deng, Z., Luong, T., Schuh, H., nn, c., & dd, e. (2022). Improving classification performance of continuous GNSS stations using a combination of Human and Machine Learning. 2nd Symposium of IAG (International Association of Geodesy) Commission 4 "Positioning and Applications" 5194. https://doi.org/10.5194/iag-comm4-2022-20

Le, N., Männel, B., Jarema, M., Seemala, G. K., Heki, K., & Schuh, H. (2021). Selection of an optimal algorithm for outlier detection in GNSS time series. *EGU General Assembly, 2021*, 5194. https://doi.org/10.5194/egusphere-egu21-1598

Legrand, J., & Bruyninx, C. (2020). Quality assessment of GNSS reference stations: Criteria and Thresholds. *Egu, 2020*, 20320. https://doi.org/10.5194/egusphere-egu2020-20320

Lehmkuhl, F., Pötter, S., Pauligk, A., & Bösken, J. (2018). Loess and other Quaternary sediments in Germany. *Journal of Maps, 14*(2), 330–340. https://doi.org/10.1080/17445647.2018.1473817

Mannel, B., Brandt, A., Bradke, M., Sakic, P., Brack, A., & Nischan, T. (2021). GFZ repro3 product series for the International GNSS Service (IGS). https://doi.org/10.5880/GFZ.1.1.2021.001

Männel, B., Brandt, A., Bradke, M., Sakic, P., Brack, A., & Nischan, T. (2020). Status of IGS reprocessing activities at GFZ.

International Association of Geodesy Symposia, 152, 37–43. https://doi.org/10.1007/1345_2020_98

Männel, B., Dobslaw, H., Dill, R., Glaser, S., Balidakis, K., Thomas, M., & Schuh, H. (2019). Correcting surface loading at the observation level: impact on global GNSS and VLBI station networks. *Journal of Geodesy, 93*(10), 2003–2017. https://doi.org/10.1007/s00190-019-01298-y

Martel, A. R. (2016). The detection of outliers in nondestructive integrations with the generalized extreme studentized deviate test. *Publications of the Astronomical Society of the Pacific, 127*(949), 258–265. https://doi.org/10.1086/680382

McCue, K. (2004). Australia: Historical earthquake studies. *Annals of Geophysics, 47*, 2–3. https://doi.org/10.4401/ag-3308

Meschede, M., & Warr, L. N. (2019). *The Geology of Germany: A process-oriented approach*. Springer. https://doi.org/10.1007/978-3-319-76102-2_12

Nickschick, T. (2017). Palaeovolcanic and present magmatic structures along the N-S trending Regensburg-Leipzig-Rostock zone kumulative Dissertation. (Doctoral dissertation). Retrieved from. https://gfzpublic.gfz-potsdam.de/rest/items/item_2016911_7/component/file_2140888/content

Nocquet, J. M., & Calais, E. (2003). Crustal velocity field of western Europe from permanent GPS array solutions, 1996–2001. *Geophysical Journal International, 154*(1), 72–88. https://doi.org/10.1046/j.1365-246X.2003.01935.x

Nocquet, J. M., Sue, C., Walpersdorf, A., Tran, T., Lenôtre, N., Vernant, P., & Van Der Beek, P. A. (2016). Present-day uplift of the western Alps. *Scientific Reports, 6*(June), 1–6. https://doi.org/10.1038/srep28404

Oliver, J. (1991). Seismology, the plate tectonics revolution, and making it happen again. *Tectonophysics, 187*(1–3), 37–49. https://doi.org/10.1016/0040-1951(91)90411-K

Petit, G., & Luzum, B. (eds). (2010). IERS Conventions. Verlag des Bundesamts für Kartographie und Geodäsie Frankfurt am Main. http://www.iers.org/TN36/

Piña-Valdés, J., Socquet, A., Beauval, C., Doin, M. P., D'Agostino, N., & Shen, Z. K. (2022). 3D GNSS velocity field sheds light on the deformation mechanisms in Europe: Effects of the vertical crustal motion on the distribution of seismicity. *Journal of Geophysical Research: Solid Earth, 127*(6), 1–25. https://doi.org/10.1029/2021JB023451

Pintori, F., Serpelloni, E., & Gualandi, A. (2022). Common-mode signals and vertical velocities in the greater Alpine area from GNSS data. *Solid Earth, 13*(10), 1541–1567. https://doi.org/10.5194/se-13-1541-2022

Place, J., Diraison, M., Naville, C., Géraud, Y., Schaming, M., & Dezayes, C. (2010). Decoupling of deformation in the Upper Rhine Graben sediments. Seismic reflection and diffraction on 3-component Vertical Seismic Profiling (Soultz-sous-Forêts area). *Comptes Rendus–Geoscience, 342*(7–8), 575–586. https://doi.org/10.1016/j.crte.2010.01.001

Raab, T., Hürkamp, K., & Völkel, J. (2010). Stratigraphy and chronology of late quaternary floodplain sediments in a historic mining area, Vils River Valley, East Bavaria, Germany. *Physical Geography, 31*(4), 357–384. https://doi.org/10.2747/0272-3646.31.4.357

Raab, T., Leopold, M., & Völkel, J. (2007). Character, age, and ecological significance of Pleistocene periglacial slope deposits in Germany. *Physical Geography, 28*(6), 451–473. https://doi.org/10.2747/0272-3646.28.6.451

Rabbel, W., Forste, K., Schulze, A., Bittner, R., Rohi, J., & Reicher, J. (1995). *A high-velocity layer in the lower crust of the North German Basin*. Terra Nova. https://doi.org/10.1111/j.1365-3121.1995.tb00802.x

Reicherter, K., Froitzheim, N., Jarosiński, M., Badura, J., Franzke, H. J., Hansen, M., & Zuchiewicz, W. (2008). Alpine tectonics north of the Alps. *Central Europe, 2*, 1233–1285. https://doi.org/10.1144/cev2p.7

Reicherter, K., Kaiser, A., & Stackebrandt, W. (2005). The postglacial landscape evolution of the North German Basin: Morphology, neotectonics and crustal deformation. *International Journal of Earth Sciences, 94*(5–6), 1083–1093. https://doi.org/10.1007/s00531-005-0007-0

Ritter, J. R., Jordan, M., Christensen, U. R., & Achauer, U. (2001). A mantle plume below the Eifel volcanic fields, Germany. *Earth and Planetary Science Letters, 186*(1), 7–14. https://doi.org/10.1016/S0012-821X(01)00226-6

Rovida, A., Antonucci, A., & Locati, M. (2022). The European preinstrumental earthquake catalogue EPICA, the 1000–1899 catalogue for the European seismic hazard model 2020. *Earth System Science Data, 14*(12), 5213–5231. https://doi.org/10.5194/essd-14-5213-2022

Rózsa, S., Heck, B., Mayer, M., Seitz, K., Westerhaus, M., & Zippelt, K. (2005). Determination of displacements in the upper Rhine graben Area from GPS and leveling data. *International Journal of Earth Sciences, 94*(4), 538–549. https://doi.org/10.1007/s00531-005-0478-z

Sánchez, L., Völksen, C., Sokolov, A., Arenz, H., & Seitz, F. (2018). Present-day surface deformation of the Alpine region inferred from geodetic techniques. *Earth System Science Data, 10*(3), 1503–1526. https://doi.org/10.5194/essd-10-1503-2018

Schmidt, A., Nowaczyk, N., Kämpf, H., Schüller, I., Flechsig, C., & Jahr, T. (2013). Origin of magnetic anomalies in the large Ebersbrunn diatreme, W Saxony, Germany. *Bulletin of Volcanology, 75*(12), 1–18. https://doi.org/10.1007/s00445-013-0766-6

Serpelloni, E., Cavaliere, A., Martelli, L., Pintori, F., Anderlini, L., Borghi, A., & Cacciaguerra, S. (2022). Surface velocities and strain-rates in the Euro-Mediterranean region from massive GPS data processing. *Frontiers in Earth Science, 10*, 1–21. https://doi.org/10.3389/feart.2022.907897

Stosch, H., Schmucker, A., & Reys, C. (1992). The nature and geological history of the deep crust under the Eifel, Germany. *Terra Nova, 4*(1), 53–62. https://doi.org/10.1111/j.1365-3121.1992.tb00450.x

Strozyk, F., Reuning, L., Scheck-Wenderoth, M., & Tanner, D. (2017). *The tectonic history of the Zechstein basin in the Netherlands and Germany*. Elsevier Inc. https://doi.org/10.1016/b978-0-12-809417-4.00011-2

Tyagunov, S., Grünthal, G., Wahlström, R., Stempniewski, L., & Zschau, J. (2006). Seismic risk mapping for Germany. *Natural Hazards and Earth System Sciences, 6*(4), 573–586. https://doi.org/10.5194/nhess-6-573-2006

Vinutha, H. P., Poornima, B., & Sagar, B. M. (2018). Detection of outliers using interquartile range technique from intrusion dataset. In J. Kacprzyk (Ed.), *Advances in intelligent systems and computing* (6th ed., pp. 511–518). Springer Nature Singapore Pte Ltd. https://doi.org/10.1007/978-981-10-7563-6

Wessel, P. (2011). Plate tectonics: Continental drift and mountain building. *Encyclopedia of Earth Sciences Series, Part, 2*, 801–812. https://doi.org/10.1016/B978-044452748-6.00101-2

Xiong, J., Wang, Q., Wan, J., Ye, B., Xu, W., & Liu, J. (2013). Detection of outliers in sensor data based on adaptive moving average fitting. *Sensor Letters, 11*(5), 877–882. https://doi.org/10.1166/sl.2013.2657

Yu, J., Meng, X., Yan, B., Xu, B., Fan, Q., & Xie, Y. (2020). Global Navigation Satellite System-based positioning technology for structural health monitoring: A review. *Structural Control and Health Monitoring*. https://doi.org/10.1002/stc.2467

Zeiß, J., Stange, S., & Brüstle, A. (2022). *Regional model of peak ground motion in Southwestern Germany* (6th ed., Vol. 26). Springer Netherlands. https://doi.org/10.1007/s10950-022-10114-8

Zhang, M., Li, X., & Wang, L. (2019). An adaptive outlier detection and processing approach towards time series sensor data. *IEEE Access, 7*, 175192–175212. https://doi.org/10.1109/ACCESS.2019.2957602

Ziegler, P. A. (1992). European Cenozoic rift system. *Tectonophysics, 208*(1–3), 91–111. https://doi.org/10.1016/0040-1951(92)90338-7